Analyst

Bioimaging using bipolar electrochemical microscopy improved in spatial resolution

Journal:	*Analyst*
Manuscript ID	AN-ART-05-2020-000912.R1
Article Type:	Paper
Date Submitted by the Author:	07-Jul-2020
Complete List of Authors:	Iwama, Tomoki; Graduate School of Environmental Studies, Tohoku University Inoue, Kumi; Graduate School of Environmental Studies, Tohoku University Abe, Hiroya; Frontier Research Institute for Interdisciplinary Sciences, Tohoku University Matsue, Tomokazu; Center for Promotion of Innovation Strategy, Tohoku University Shiku, Hitoshi ; Graduate School of Environmental Studies, Tohoku University

SCHOLARONE™
Manuscripts

Please do not adjust margins

ARTICLE

Bioimaging using bipolar electrochemical microscopy improved in spatial resolution

Received 00th January 20xx,
Accepted 00th January 20xx

DOI: 10.1039/x0xx00000x

Tomoki Iwama,[a] Kumi Y. Inoue,*[a] Hiroya Abe,[b] Tomokazu Matsue[c] and Hitoshi Shiku*[a]

In this study, we developed a bipolar electrochemical microscopy (BEM) using a closed bipolar electrode (cBPE) array with an electrochemiluminescence (ECL) detecting system. Because cBPEs are not directly connected to a detector, high spatio-temporal resolution imaging can be achieved by fabricating a microelectrode array where each electrode point is arranged in a short interval. A cBPE array with individual cBPEs arranged in 41 µm intervals was successfully fabricated by depositing gold in the pores of a track-etched membrane using electroless plating. Using BEM with the cBPE array, which has a higher density of electrode points than the conventional multi-electrode array, we effectively demonstrated the imaging of $[Fe(CN)_6]^{3-}$ diffusion and the respiratory activity of the MCF-7 spheroids with high spatio-temporal resolution.

Introduction

Bioimaging technologies have considerably contributed to the fields of life science and therapeutic researches providing knowledge about functions of biological samples including cells and living tissues. Optical observation methods combined with various fluorescent probes have been developed for bioimaging as well as other imaging techniques such as positron emission tomography (PET) and nuclear magnetic resonance (NMR) spectroscopy. Among these bioimaging technologies, electrochemical imaging has the advantages of being non-invasive and label-free to biological samples[1, 2]. Scanning electrochemical microscopy (SECM) is a major electrochemical imaging method at the single-cell scale providing a highly spatial resolution[1, 3, 4]. However, SECM is not suitable to track fast biological phenomena of a large area because SECM requires tens of minutes of measurement time to scan with a microelectrode probe. The multi-electrode array (MEA) method, another electrochemical imaging method, has the advantage of high temporal resolution[5-6]. The real-time imaging of wide-scale biological signals, such as a rat hippocampal tissue slice[7], embryo bodies[8], and neuron-like cell spheroids[9], have been achieved using electrochemical imaging techniques. However, conventional multi-electrode arrays require connecting lines between the voltage supplier and individual microelectrodes, which severely limits the spatial resolution of the resulting electrochemical images. Therefore, it is challenging for the conventional multi-electrode arrays to observe the local biological phenomena such as the metabolism of cardiomyocytes and the synaptic communication between individual nerve cells. Moreover, the conventional multi-electrode arrays are expensive due to the photolithographic process fabricating a device.

To overcome these problems, our group has proposed bipolar electrochemical microscopy (BEM) for the highly spatio-temporal resolution imaging (Fig. 1). The BEM consists of a closed bipolar electrode (cBPE) array and a pair of driving electrodes. By applying a sufficient voltage bias between the driving electrodes in the solutions separated by the cBPE array, electrochemical reactions are simultaneously induced at the poles of the cBPE without direct connection from an external power generator to each cBPE. High spatio-temporal resolution imaging by BEM can be achieved using a high-density cBPE array in combination with an electrochemiluminescence (ECL) reporting system. We previously reported a first BEM concept with a cBPE array fabricated using manually bundled 300 µm-diameter gold wires[10]. In the study, we successfully proved the basic principle of the BEM obtaining an image of flowing $[Fe(CN)_6]^{3-}$. In a similar study, Zhang's group reported the fluorescence-enabled electrochemical microscopy (FEEM) applying the principle of bipolar electrochemistry for chemical imaging. Using a carbon fiber electrode array and fluorescence signal, they achieved the imaging of $[Fe(CN)_6]^{3-}$ diffusion[11]. Eßmann et al. reported the scanning bipolar electrochemical microscopy (SBECM) system, which enables either high spatial resolution or high temporal resolution imaging by accumulating or monitoring the ECL signal while scanning the bipolar electrode array probe[12]. Recently, Anderson et al. achieved the high spatio-temporal resolution imaging of $[Fe(CN)_6]^{3-}$ using the principle of cBPE and ECL[13]. The ECL signal realizes a higher S/N

[a] Graduate School of Environmental Studies, Tohoku University, Sendai, Miyagi, Japan.
[b] Frontier Research Institute for Interdisciplinary Sciences, Tohoku University, Sendai, Miyagi, Japan.
[c] Center for Promotion of Innovation Strategy, Tohoku University, Sendai, Miyagi, Japan.
*Corresponding authors:
Kumi Y. Inoue Tel: +81-22-752-2209 E-mail: kumi.inoue.b3@tohoku.ac.jp
Hitoshi Shiku Tel: +81-22-795-7209 E-mail: hitoshi.shiku.c3@tohoku.ac.jp

Please do not adjust margins

ratio detection in comparison with the fluorescence signal because of its background-signal free feature. Moreover, the observation of an ECL signal does not require a large device, such as an excitation light source, which is needed for the observation of the fluorescence signal. From these advantages, detection system[14,15] and microscopy systems[15-19] capable of single cell analysis using ECL has been reported. However, there are no reports that describe high spatial-temporal resolution imaging using the principle of cBPE and ECL, which can prevent biological samples from being exposed to luminophore solutions, to observe biological activity from changes of extracellular concentrations of substances that cells uptake from and release into the external environment.

Herein, we report a highly improved BEM with a spatial resolution of 41 µm pitch and a temporal resolution of 100 ms. A cBPE array was fabricated via electroless plating on a micropore membrane[20-25] without any photolithographic technique. This cBPE array fabrication method has the potential to enable higher spatial resolution imaging by applying it to a finer porous membrane. A flow image of $[Fe(CN)_6]^{3-}$ in solution was observed by the BEM to evaluate the device performance. Then, we demonstrated the bioimaging of the respiratory activity of the MCF-7 spheroids by mapping the oxygen concentration using BEM.

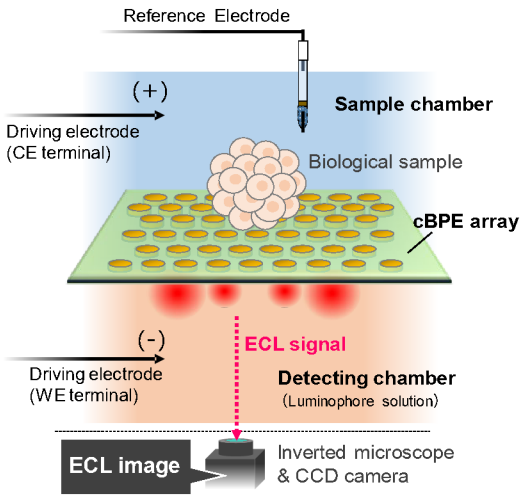

Figure 1. Schematic illustration of BEM.

Figure 1 shows the system configuration of BEM. The sample was accommodated in a sample chamber, and the ECL signal was detected through a detecting chamber containing a luminophore solution. The sample chamber and the detecting chamber were separated by a cBPE array and there is no mixing of both solutions. A reference electrode (RE; Ag/AgCl sat. KCl) was inserted into the sample chamber. A Pt driving electrode connected to the counter electrode (CE) terminal of a potentiostat was placed in the sample chamber, and another Pt driving electrode connected to the working electrode (WE) terminal of the potentiostat was placed in the detecting chamber. By applying a negative voltage on the driving electrode of the WE terminal, reduction and oxidation reactions were generated at the poles of the sample chamber and detecting chamber sides of the cBPE, respectively. Target molecules were imaged using a CCD camera, which detected the ECL signal generated from the oxidation of the luminophore molecules on the surface of the cBPE in the detecting chamber corresponding to the reduction of the target molecules on the other surface of the cBPE in the sample chamber, under the condition that the target molecule reduction reaction was the limiting process of the whole electrochemical reaction system.

Results and discussion

Fabrication of cBPE array. The cBPE array was fabricated by the electroless plating of the micropores of the track-etched membrane (Cell Culture Inserts; Falcon®) using a gold ion solution ($HAuCl_4$) and reducing agent ($NaBH_4$) [25] (Fig. 2A). The track-etched membrane is a microporous membrane made of polyethylene terephthalate. The pores with a diameter of 8 µm are opened almost vertically, therefore, the pores rarely intersect each other inside the membrane. An aliquot of 50 mM $HAuCl_4$ (in water) and 50 mM $NaBH_4$ solution (in EtOH) were separated by the track-etched membrane for 30 min to induce the gold deposition reaction in the micropores. The extraneous deposits on the surface of the track-etched membrane were removed using a cotton swab. The deposition and the swab were repeated until the gold completely filled the micropores. This was verified using with an optical microscope. Figure 2B and 2C show the surface of the track-etched membrane before and after applying a series of fabrication methods of the cBPE array. The gold filling of each micropore was confirmed, proving that the cBPE array was successfully fabricated. The track-etched membrane has an average pore interval of 41 µm ($6\pm2\times10^4/cm^2$, according to product information). When the densities of pores and BPE were counted from Fig. 2B and 2C, they were $7.93 \times 10^4/cm^2$ and $5.40 \times 10^4/cm^2$, respectively. The average spacing between the pore and BPE was calculated for each of these values and found to be 35 µm and 43 µm pitch on average, respectively. This difference in density between Fig 2B and 2C is due to the variation in the distribution of holes in the track-etched membrane, indicating that the spatial resolution may differ depending on the area. The problem of this variation in distribution can be solved by using a more finely arranged porous membrane. However, the values for these intervals are considerably higher than the 500 µm pitch of the cBPE array reported previously[10]. The reproducibility of cBPE array is not 100% due to short circuits between electrodes by unwanted gold adsorption. In addition, the ion leak largely influences to the homogeneity and reproducibility of the BEM. It is difficult to control the cause of these problem, however, the complete cBPE array (though the yield is not 100%) can be used with high probability. The highly reproducible method to make cBPE array is an issue to be studied in the future. Regarding crosstalk, when electrodes with a diameter of 8 um are arrayed at a pitch of 41 um, diffusion layers do not overlap theoretically.

This journal is © The Royal Society of Chemistry 20xx

Please do not adjust margins

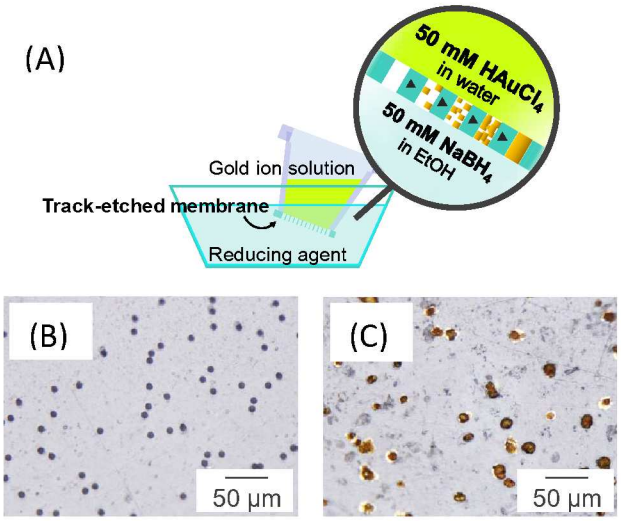

Figure 2. (A) Schematic of cBPE array fabrication using electroless plating method with gold. Optical microscope image of the surface of the track-etched membrane (B) before and (C) after electroless plating of gold.

Demonstration of high spatio-temporal resolution imaging. The imaging of the molecule flow in solution was demonstrated using the BEM with the cBPE array. The edges of the cBPE array were covered with epoxy resin so that the observation area fits within the field of view of the camera. A 0.1 M KCl solution was poured into the sample chamber. A mixed solution of 10 mM $[Ru(bpy)_3]Cl_2$ and 100 mM tripropylamine (TPA) containing 0.1 M KCl was added to the detecting chamber. Applying -1.1 V to the WE as the driving voltage and observing the ECL signal by a CCD camera (gain: 255, exposure time: 100 ms), 500 µL of the 50 mM potassium ferricyanide ($K_3[Fe(CN)_6]$) solution (containing 0.1 M KCl) was injected into the sample chamber. Figure 3 shows the time-lapse images of the ECL signals obtained during injection of the $K_3[Fe(CN)_6]$ solution. The ECL signals conjugated to the reduction of the $[Fe(CN)_6]^{3-}$ molecules demonstrated the spreading activity of $[Fe(CN)_6]^{3-}$ on the cBPE array on the sample chamber side. A series of ECL images were obtained in 100 ms intervals. Individual ECL signals were released from each point of the cBPEs, which were placed at an average interval of 41 µm. The ECL signals, which coupled with the reduction reaction of the analyte, increased with the $[Fe(CN)_6]^{3-}$ concentration on each cBPE. These results demonstrate the capability of the BEM using a cBPE array fabricated by electroless plating of a track-etched membrane for high spatio-temporal resolution imaging of the sample molecules. The image in Fig. 3 has large and small signals, and there is a possibility that the signal intensity of each BPE is uneven. This is considered to be the effect of ion contacts in gold and needs further improvement.

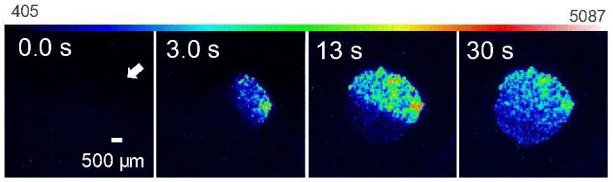

Figure 3. Time-lapse images of the high spatio-temporal resolution ECL signal of $[Fe(CN)_6]^{3-}$ solution spreading on the cBPE array in the sample chamber. Gain 255, exposure time 100 ms.

Detection of oxygen. To apply this BEM to observe biological phenomena, an imaging of the respiratory activity of the MCF-7 spheroids was performed. To determine the driving voltage required to detect oxygen in the sample chamber as the ECL signal, the relationship between the oxygen concentration and the intensity of the ECL signal derived from the reduction of oxygen in the sample chamber was examined. Phosphate-buffered saline (PBS) containing 10 mM $[Ru(bpy)_3]Cl_2$ and 100 mM TPA was added to the detecting chamber. The sample chamber was filled with untreated PBS (containing 0.258 mM O_2 at 24.0 °C), O_2-saturated PBS (containing 1.23 mM O_2 at 24.0 °C), or Ar-saturated PBS (containing no O_2 at 24.5 °C). The potential between the driving electrodes was swept between 0.0 and -3.0 V at a scan rate of 50 mV s^{-1}, and the ECL signal was observed by the CCD camera (gain: 255, exposure time: 100 ms). Figure 4 shows the sum of the ECL signal intensity obtained from the entire cBPE array against the driving voltage. The ECL signal increased at a voltage lower than -2.0 V using untreated and O_2-saturated PBS as samples. Comparing the two conditions, the ECL signal obtained with the O_2-saturated PBS was 2.0–2.2 times higher than that obtained with the untreated PBS. In contrast, the ECL signals obtained with Ar-saturated PBS showed no significant increase. These results indicated that the oxygen reduction reaction on the cBPEs in the sample chamber together with the ECL signal release in the detecting chamber started at -2.0 V, and the ECL signal intensity depended on the oxygen concentration in the sample solution. The required driving voltage of -2.0 V is explained as a difference between the required potential for oxygen reduction (-0.6 V vs. Ag/AgCl) and the required potential for ECL generation by $Ru(bpy)_3^{2+}$/TPA oxidation (+0.8 V vs. Ag/AgCl) [26] plus an excessive voltage of 0.6 V required to compensate for voltage drop due to ion current from a slight presence of ion junction in the gold electrode. The reason that the oxygen concentration and the ECL intensity were not proportional was that the oxygen leaking to the luminophore side through a slight ion junction in the gold electrode inhibits

This journal is © The Royal Society of Chemistry 20xx

Please do not adjust margins

the ECL generation reaction[27]. The another possible reason is that the oxygen concentration in the solution was reduced before the measurement after transferring the oxygen-bubbled PBS to the chamber.

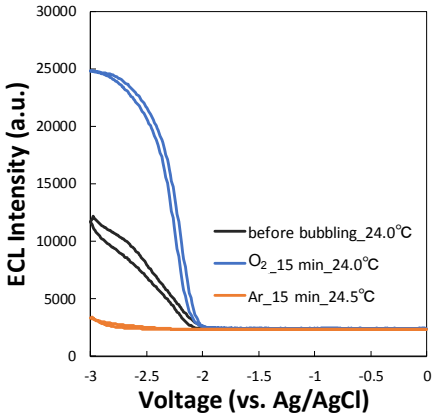

Figure 4. ECL intensities measured while sweeping the driving voltage on WE. (Black) PBS without gas bubbling, (blue) after O_2 gas bubbling for 15 min, and (red) after Ar gas bubbling for 15 min.

Imaging of respiration activity of MCF-7 spheroids. To image the respiration activity of the MCF-7 spheroids, the O_2 consumption of MCF-7 spheroids was evaluated using BEM. The MCF-7 spheroids were prepared by the hanging drop method. Approximately 1000 cells were cultured for 5 days at 37 °C in a 20 µL droplet of a culture medium. To stop the respiration of MCF-7 spheroids, one spheroid was soaked in 4% paraformaldehyde for 30 min and then washed twice with PBS. The PBS was filled into the sample chamber, and the PBS containing 10 mM $[Ru(bpy)_3]Cl_2$ and 100 mM TPA was added to the detecting chamber. After both paraformaldehyde-treated and non-treated spheroids were placed on the cBPE array (Fig. 5A), -2.6 V was applied to the WE as the driving voltage while observing the ECL signal with the CCD camera (gain: 255, exposure time: 100 ms). As a result, the ECL signal around the live cell spheroid decreased more than that around the dead cell spheroid, although the ECL signal around both the dead and live cell spheroids decreased (Fig. 5B). The reason why an ECL signal decrease was observed for the dead spheroid, even though this spheroid had no respiration activity, is the physical inhibition of oxidant diffusion to the cBPE surface. Because the living spheroid consumed oxygen by respiration, the ECL signal decreased significantly more, in addition to the physical diffusion inhibition. The size of the spheroids used in this experiment is slightly different (living spheroid 259 µm, dead spheroid 210 µm), and the effect of oxygen diffusion inhibition may be different. We evaluated the effect of oxygen diffusion inhibition by simulations (COMSOL Multiphysics), and the difference in area size of ECL elimination in the Fig. 5B was not only due to the difference in diffusion inhibition, but also due to the consumption of oxygen by living spheroids. Details are shown in supplementary information. These results confirmed the successful monitoring of respiration activity of MCF-7 spheroids using BEM. However, a platinum electrode, which produces a smaller amount of hydrogen peroxide during oxygen reduction, is more suitable for evaluating the oxygen concentration in a biological sample. It is necessary to study electrode materials in the future in order to perform highly sensitive evaluation with less damage to biological samples. The imaging or evaluation of the respiration activity of cell spheroids was achieved by the conventional multi-electrode array method or the detecting device using cBPE and ECL[28]. The BEM used in this study obtained 2D information of the cell respiration activity with higher spatial resolution.

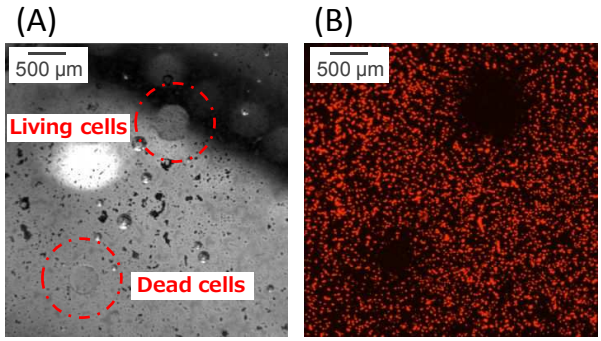

Figure 5. (A) Position of the spheroid recorded from below the detecting chamber with the CCD camera. (B) ECL image obtained by applying -2.6 V on WE with live/dead cells on the cBPE array surface.

Experimental

Chemicals

KCl, EtOH, $K_3[Fe(CN_6)]$, $NaBH_4$, TPA, and PBS (Dulbecco's PBS) were purchased from Wako Pure Chemical Industries, Japan. $HAuCl_4 \cdot 4\ H_2O$ was purchased from KISHIDA CHEMICAL Co., Ltd., Japan. $[Ru(bpy)_3]Cl_2$ was purchased from Tokyo Chemical Industry Co., Ltd., Japan.

Instruments and software

Compactstat (Ivium) was used as a potentiostat for all the electrochemical measurements. The PI-MAX CCD camera (Princeton Instruments) and Winspec 32 imaging software (Princeton Instruments) were used to observe the spreading activity of the $[Fe(CN)_6]^{3-}$ solution. The ImagEM X2 CCD camera (Hamamatsu Photonics K.K.) and HCImage Live imaging software (Hamamatsu Photonics K.K.) were used in the experiments to determine the oxygen detection voltage and observe the respiratory activity of the MCF-7 spheroids.

This journal is © The Royal Society of Chemistry 20xx

Fabrication of cBPE

Track-etched membrane made of polyethylene terephthalate (Cell Culture Inserts) was purchased by Corning (USA). The trach-etched membrane has 8 µm pores randomly formed in the density of $6\pm2\times10^4/cm^2$. An aliquot of 50 mM $HAuCl_4$ (in water) and 50 mM $NaBH_4$ solution (in EtOH) were separated by the track-etched membrane for 30 min to induce the gold deposition reaction in the micropores. The extraneous deposits on the surface of the track-etched membrane were removed using a cotton swab. The deposition and the swab were repeated until the gold filled the micropores without any mixing of solutions. In the measurement, the edges of the cBPE array were covered with epoxy resin so that the observation area fits within the field of view of the camera.

Fabrication of driving electrodes

The driving electrodes were fabricated using the photolithography and sputtering technique. Pt was sputtered on the glass plate (S-1127; MATSUNAMI). After sputtering Pt and cutting to the appropriate size, the electrode area was defined with SU-8 negative photoresist (KAYAKU Advanced Materials, Inc.). The 8 cm^2 driving electrodes were used for the observation of the spreading activity of the $[Fe(CN)_6]^{3-}$ solution. The 24 mm^2 driving electrodes were used to determine the oxygen detection voltage and to observe the respiratory activity of the MCF-7 spheroids.

Preparation of MCF-7 spheroids

MCF-7 cells were purchased from the Institute of Development, Aging and Cancer at Tohoku University (Japan). The MCF-7 spheroids were cultured by a hanging drop method. Approximately 20 µL of droplets of a culture medium containing 1000 cells were hung on dish covers and cultured for 5 days. The control sample to observe the respiratory activity, which was shown in Fig. 5 as dead cells, was immersed in 4% paraformaldehyde (Wako Pure Chemicals Ltd.) for 30 min to stop the respiratory activity.

Conclusions

In conclusion, BEM was developed to realize high spatio-temporal resolution bio-imaging by fabricating a cBPE array on a micropore membrane using electroless plating. The flow of $[Fe(CN)_6]^{3-}$ on the cBPE array was successfully monitored in high spatio-temporal resolution. In addition, the applicability for bio-imaging was demonstrated by observing the difference in the respiratory activity of the living and dead MCF-7 spheroids and imaging the oxygen concentration on the cBPE array. This novel imaging system has the potential to be used as a microsco observe various biological phenomena.

Conflicts of interest

There are no conflicts to declare.

Acknowledgements

This research was supported by Grant-in-Aid for Scientific Research (C) (no. 19K05687), Grant-in-Aid for Young Scientists (no. 19K15598), and Grant-in-Aid for JSPS Fellows (no. 19J20709) from Japan Society for the Promotion of Science (JSPS). It also partially supported by JST COI (no. JPMJCE1303) from Japan Science and Technology Agency (JST).

Notes and references

1 K. Ino, M. Şen, H. Shiku and T. Matsue, *Analyst*, 2017, **142**, 4343.
2 T. E. Lin, S. Rapino, H. H. Girault and A. Lesch, *Chem. Sci.*, 2018, **9**, 4546.
3 S. Amemiya, A. J. Bard, F.-R. F. Fan, M. V. Mirkin and P. R. Unwin, *Annu. Rev. Anal. Chem.*, 2008, **1**, 95.
4 H. Shiku, T. Shiraishi, H. Ohya, T. Matsue, H. Abe, H. Hoshi and M. Kobayashi, *Anal. Chem.*, 2001, **73**, 3751.
5 N. Kasai, Y. Jimbo and K. Torimitsu, *Anal. Sci.*, 2002, **18**, 1325.
6 H. Abe, T. Iwama, H. Yabu, K. Ino, K. Y. Inoue, A. Suda, R. Kunikata, M. Matsudaira and T. Matsue, *Electroanalysis*, 2018, **30**, 2841.
7 N. Kasai, Y. Jimbo, O. Niwa, T. Matsue and K. Torimitsu, *Neurosci. Lett.*, 2001, **304**, 112.
8 Y. Kanno, K. Ino, K. Y. Inoue, A. Suda, R. Kunikata, M. Matsudaira, H. Shiku and T. Matsue, *Anal. Sci.*, 2015, **31**, 715.
9 H. Abe, K. Ino, C.-Z. Li, Y. Kanno, K. Y. Inoue, A. Suda, R. Kunikata, M. Matsudaira, Y. Takahashi, H. Shiku and T. Matsue, *Anal. Chem.*, 2015, **87**, 6364.
10 T. Iwama, K. Y. Inoue, H. Abe and T. Matsue, *Chem. Lett.*, 2018, **47**, 843.
11 S. M. Oja and B. Zhang, *Anal. Chem.*, 2014, **86**, 12299.
12 V. Eßmann, C. Santana Santos, T. Tarnev, M. Bertotti and W. Schuhmann, *Anal. Chem.*, 2018, **90**, 6267.
13 T. J. Anderson, P. A. Defnet and B. Zhang, *Anal. Chem.*, 2020, acs.analchem.0c00921.
14 Y. Wang, R. Jin, N. Sojic, D. Jiang and H.-Y. Chen, *Angew. Chem. Int. Ed.*, 2020, **59**, 1.
15 K. Hiramoto, E. Villani, T. Iwama, K. Komatsu, S. Inagi, K. Y. Inoue, Y. Nashimoto, K. Ino, and H. Shiku, *Micromachines*, 2020, 11, 530; doi:10.3390/mi11050530
16 G. Valenti, S. Scarabino, B. Goudeau, A. Lesch, M. Jović, E. Villani, M. Sentic, S. Rapino, S. Arbault, F. Paolucci and N. Sojic, *J. Am. Chem. Soc*, 2017, **139**, 16830.
17 S. Voci, B. Goudeau, G. Valenti, A. Lesch, M. J. Jović, S. Rapino, F. Paolucci, S. S. Arbault and N. Sojic, *J. Am. Chem. Soc*, 2018, **140**, 14753.
18 J. Zhang, R. Jin, D. Jiang and H.-Y. Chen, *J. Am. Chem. Soc*, 2019, **141**, 10294.
19 H. Ding, W. Guo and B. Su, *Angew. Chem. Int. Ed.*, 2020, **59**, 449.
20 H. Zhang, X. Hou, J. Hou, L. Zeng, Y. Tian, L. Li and L. Jiang, *Adv. Funct. Mater.*, 2015, **25**, 1102.
21 M. Nishizawa, V. P. Menon and C. R. Martin, *Science*, 1995, **268**, 700.
22 V. P. Menon, C. R. Martin, *Anal. Chem.*, 1995, **67**, 1920.
23 C. R. Martin, *Chem. Mater*, 1996, **8**, 1739.
24 H. B. Habtamu, M. Sentic, M. Silvestrini, L. De Leo, T. Not, S. Arbault, D. Manojlovic, N. Sojic and P. Ugo, *Anal. Chem.*, 2015, **87**, 12080.
25 Q. Zhai, X. Zhang, Y. Han, J. Zhai, J. Li and E. Wang, *Anal. Chem.*, 2016, **88**, 945.
26 W. Miao, J. P. Choi, and A. J. Bard, *J. Am. Chem. Soc.*, 2002, 124, 14478.
27 H. Zheng and Y. Zu, *J. Phys. Chem. B*, 2005, **109**, 12049.
28 K. Ino, R. Yaegaki, K. Hiramoto, Y. Nashimoto and H. Shiku, *ACS Sensors*, 2020, **5**, 740.

This journal is © The Royal Society of Chemistry 20xx